

Attention-aware Post-training Quantization without Backpropagation

Junhan Kim, Ho-young Kim, Eulrang Cho, Chungman Lee, Joonyoung Kim, Yongkweon Jeon
Samsung Research

{jun_one.kim, hoyoung4.kim, eulrang.cho, chungman.lee, joon5369.kim, dragwon.jeon}@samsung.com

Abstract

Quantization is a promising solution for deploying large-scale language models (LLMs) on resource-constrained devices. Existing quantization approaches, however, rely on gradient-based optimization, regardless of it being post-training quantization (PTQ) or quantization-aware training (QAT), which becomes problematic for hyper-scale LLMs with billions of parameters. This overhead can be alleviated via recently proposed backpropagation-free PTQ methods; however, their performance is somewhat limited by their lack of consideration of inter-layer dependencies. In this paper, we thus propose a novel PTQ algorithm that considers inter-layer dependencies without relying on backpropagation. The fundamental concept involved is the development of attention-aware Hessian matrices, which facilitates the consideration of inter-layer dependencies within the attention module. Extensive experiments demonstrate that the proposed algorithm significantly outperforms conventional PTQ methods, particularly for low bit-widths.

1 Introduction

The explosive growth in complexity (parameters) of large-scale language models (LLMs) (Touvron et al., 2023; Zhang et al., 2022) has resulted in a proportional increase in computational costs, which has prompted an urgent need for efficient model processing and compression strategies. Quantization has emerged as a pivotal solution in this context, and it serves as an essential step in the deployment of AI models on resource-constrained devices that primarily support fixed-point arithmetic. By reducing precision, the memory bandwidth requirements can be alleviated, and the significant parallelism of quantized models can be SIMDified using highly efficient vector processing units, such as neural processing unit (NPU).

Two main categories of quantization approaches have been proposed to preserve the performance

of original full-precision models: quantization-aware training (QAT) and post-training quantization (PTQ). Although QAT can potentially outperform PTQ, its practicality diminishes considerably when handling hyper-scale LLMs featuring billions of parameters. Consequently, recent quantization efforts have been directed toward PTQ.

Although classic PTQ methods have successfully quantized small-scale models (Nagel et al., 2020; Li et al., 2021), they rely on time-consuming gradient-based optimization, so their efficacy decreases when the complexity of LLMs increases. Accordingly, backpropagation-free PTQ methods have been developed for LLMs (Frantar et al., 2023; Xiao et al., 2023; Jeon et al., 2023b); however, their performance is somewhat limited owing to the lack of consideration of inter-layer dependencies. Recent studies have attempted to consider inter-layer dependencies (Shao et al., 2023; Ma et al., 2024), but they still rely on time-consuming gradient-based optimizations.

In this paper, we propose a novel quantization algorithm that considers inter-layer dependencies without relying on backpropagation. Our primary contributions can be summarized as follows:

- We propose a novel PTQ algorithm called BOA.¹ To avoid time-consuming gradient-based optimization, we adopt the Hessian-based strategy introduced by (Frantar and Alistarh, 2022). The primary novelty lies in the fact that we exploit the attention reconstruction error, not the layer-wise reconstruction error, when approximating the Hessian. This facilitates the consideration of the inter-layer dependencies within the attention module (**Section 3.1**).
- While the proposed Hessian facilitates the consideration of inter-layer dependencies, it re-

¹BOA: Backpropagation-free optimization for Attention-aware PTQ

quires a large amount of memory and high computational cost. Therefore, we incorporate several techniques to mitigate the computational overhead, including Hessian relaxation, efficient computation of inverse Hessians, and head-wise simultaneous quantization (Section 3.2).

- We evaluate BOA via extensive experiments on publicly available LLMs (Section 4). Our results demonstrate that BOA outperforms conventional LLM PTQ methods by a significant margin, particularly for low-bit precision (*e.g.*, INT2).

2 Related Works

2.1 PTQ for LLMs

When calibration data are available, PTQ primarily aims to minimize the increase in task loss incurred by quantization. Consider a neural network parameterized by weights \mathbf{W} . Provided that the network is trained to convergence, the problem of quantizing \mathbf{W} to minimize task loss degradation can be formulated as (LeCun et al., 1989)

$$\min_{\Delta \mathbf{w}} \Delta \mathbf{w}^T \cdot \mathbf{H}^{(\mathbf{w})} \cdot \Delta \mathbf{w}, \quad (1)$$

where $\mathbf{H}^{(\mathbf{w})}$ is the Hessian related to the flattened weight \mathbf{w} and $\Delta \mathbf{w}$ is a weight perturbation caused by the quantization. Owing to the infeasibility of computing and storing the exact Hessian $\mathbf{H}^{(\mathbf{w})}$, many studies have assumed independence between layers, which relaxes (1) into the following layer-wise reconstruction problem (Nagel et al., 2020):

$$\min_{\Delta \mathbf{W}^{(\ell)}} \left\| \Delta \mathbf{W}^{(\ell)} \mathbf{X}^{(\ell-1)} \right\|_F^2, \quad (2)$$

where $\mathbf{X}^{(\ell-1)}$ is the input to the ℓ -th layer parameterized by $\mathbf{W}^{(\ell)}$.

To solve (2), early efforts aimed to optimize the weight-rounding mechanisms (Nagel et al., 2020; Hubara et al., 2021; Li et al., 2021; Jeon et al., 2022, 2023a). Instead of selecting the nearest quantization bin, these studies attempted to assign quantized values that minimize layer-wise reconstruction errors. In AdaRound (Nagel et al., 2020), an algorithm for optimizing the weight-rounding mechanism through backpropagation has been proposed. Further, this algorithm has been extended to BRECQ (Li et al., 2021) to consider the inter-layer dependencies within a certain network block (*e.g.*,

Transformer block), thereby enhancing the low-bit quantization performance.

Although these algorithms have successfully quantized small-sized models such as ResNet, they are heavily dependent on time-consuming gradient-based optimizations. This renders their application to LLMs with billions of parameters challenging. Consequently, recent efforts have shifted towards the development of cost-effective quantization methods for LLMs. For example, a backpropagation-free weight-rounding method called OPTQ (or GPTQ) has been proposed (Frantar et al., 2023). Furthermore, algorithms leveraging additional “foldable” parameters capable of being integrated into other layers (*e.g.*, LayerNorm) have been proposed (Xiao et al., 2023; Lin et al., 2024; Jeon et al., 2023b; Shao et al., 2023; Ma et al., 2024). Rather than optimizing a weight-rounding mechanism, these studies focused on enhancing the performance of the nearest-rounding by suppressing activation outliers or conducting more precise quantization based on foldable parameters.

2.2 Review of OPTQ

Among the quantization methods developed for LLMs, OPTQ has been extensively focused upon owing to its efficiency. OPTQ can quantize hyper-scale LLMs with more than 30B parameters in a few GPU hours with negligible performance degradation for INT3/INT4 (Frantar et al., 2023). In addition, OPTQ can be used to boost the performance of other quantization methods that leverage foldable parameters (Lin et al., 2024; Jeon et al., 2023b; Lee et al., 2023).

In OPTQ, weights are quantized one by one according to a pre-defined order. Once a weight is quantized, OPTQ updates the remaining (not-yet-quantized) weights to compensate for the task loss degradation caused by quantization. When the q -th weight w_q is quantized, the weight-update $\delta \mathbf{w}$ is mathematically expressed as

$$\delta \mathbf{w} = -\frac{w_q - \mathcal{Q}(w_q)}{[\mathbf{U}]_{q,q}} [\mathbf{U}]_{q,:}, \quad (3a)$$

$$\mathbf{U} = \text{Chol}(\mathbf{H}^{-1})^T, \quad (3b)$$

where $\text{Chol}(\cdot)$ denotes a Cholesky decomposition (*i.e.*, \mathbf{U} is an upper triangular matrix satisfying $\mathbf{H}^{-1} = \mathbf{U}^T \mathbf{U}$). Owing to the difficulty in computing the exact Hessian \mathbf{H} , OPTQ approximates \mathbf{H} by assuming layer-wise independence. Consequently, the task loss degradation is relaxed to a

Table 1: Proposed attention-aware Hessians

Layer	H
$\mathbf{W}_{Q,h}$	$2\mathbf{X}\mathbf{X}^T \otimes \mathbf{K}_h^T \mathbf{K}_h$
$\mathbf{W}_{K,h}$	$2\mathbf{X}\mathbf{X}^T \otimes \mathbf{Q}_h^T \mathbf{Q}_h$
$\mathbf{W}_{V,h}$	$2\mathbf{X}\mathbf{A}_h^T \mathbf{A}_h \mathbf{X}^T \otimes \mathbf{W}_{\text{out},h}^T \mathbf{W}_{\text{out},h}$
$\mathbf{W}_{\text{out},h}$	$2\mathbf{X}_{\text{out},h} \mathbf{X}_{\text{out},h}^T \otimes \mathbf{I}$
\mathbf{W}_{fc1}	$2\mathbf{X}_{\text{fc1}} \mathbf{X}_{\text{fc1}}^T \otimes \mathbf{I}$
\mathbf{W}_{fc2}	$2\mathbf{X}_{\text{fc2}} \mathbf{X}_{\text{fc2}}^T \otimes \mathbf{I}$

layer-wise reconstruction error (as in (2)) (Nagel et al., 2020), which yields the following Hessian equation:

$$\mathbf{H}^{(w^{(\ell)})} \approx 2\mathbf{X}^{(\ell-1)} \mathbf{X}^{(\ell-1)T} \otimes \mathbf{I}, \quad (4)$$

where \otimes denotes the Kronecker product operation and \mathbf{I} is the identity matrix.² In Appendix D, we provide the pseudocode of the OPTQ algorithm.

As evident, the approximated Hessian relies only on the input. Therefore, OPTQ cannot consider the influence of other layers when compensating for the quantization error based on the Hessian (see (3a)). In other words, OPTQ does not consider the inter-layer dependency within the attention module, which is a key feature of Transformers. Owing to ignorance of inter-layer dependency, OPTQ exhibits somewhat limited low-bit (e.g., INT2) quantization performance (Jeon et al., 2023b). Thus, we aim to develop attention-aware Hessians, thereby incorporating the inter-layer dependencies within the attention module.

3 Method

3.1 Proposed attention-aware Hessian

To consider the inter-layer dependencies within the attention module, we exploit the attention reconstruction error rather than the layer-wise reconstruction error when approximating the Hessian.

For an input sequence $\mathbf{X} \in \mathbb{R}^{d \times L}$, the output of the multi-head attention (MHA) is expressed as

$$\text{MHA}(\mathbf{X}) = \sum_{h=1}^H \mathbf{W}_{\text{out},h} (\mathbf{A}_h \mathbf{V}_h)^T, \quad (5a)$$

$$\mathbf{A}_h = \sigma \left(\frac{\mathbf{Q}_h \mathbf{K}_h^T}{\sqrt{d_h}} \right), \quad (5b)$$

$$[\mathbf{Q}_h | \mathbf{K}_h | \mathbf{V}_h] = \mathbf{X}^T [\mathbf{W}_{Q,h}^T | \mathbf{W}_{K,h}^T | \mathbf{W}_{V,h}^T], \quad (5c)$$

where σ is the row-wise softmax function, d_h is the embedding dimension of the h -th attention head, $\mathbf{W}_{\{Q,K,V\},h} \in \mathbb{R}^{d_h \times d}$, and $\mathbf{W}_{\text{out},h} \in \mathbb{R}^{d \times d_h}$.

²For any \mathbf{M}_1 and \mathbf{M}_2 , the second-order derivative of $\|\mathbf{M}_1 \Delta \mathbf{W} \mathbf{M}_2\|_F^2$ with respect to $\Delta \mathbf{w}$ is $2\mathbf{M}_2 \mathbf{M}_2^T \otimes \mathbf{M}_1^T \mathbf{M}_1$ (see Appendix A for the proof).

Hessian for $\mathbf{W}_{Q,h}$ When $\mathbf{W}_{Q,h}$ is quantized, $\mathbf{W}_{\text{out},h}$ and \mathbf{V}_h in (5a) remain unchanged, but the attention weight \mathbf{A}_h changes. Using the first-order Taylor polynomial, the perturbation in \mathbf{A}_h can be approximated as

$$\begin{aligned} \Delta \mathbf{A}_h &= \sigma \left(\frac{(\mathbf{Q}_h + \Delta \mathbf{Q}_h) \mathbf{K}_h^T}{\sqrt{d_h}} \right) - \sigma \left(\frac{\mathbf{Q}_h \mathbf{K}_h^T}{\sqrt{d_h}} \right) \\ &\approx \frac{\Delta \mathbf{Q}_h \mathbf{K}_h^T}{\sqrt{d_h}} \mathbf{J}_\sigma^T = \frac{\mathbf{X}^T \Delta \mathbf{W}_{Q,h}^T \mathbf{K}_h^T \mathbf{J}_\sigma^T}{\sqrt{d_h}}, \end{aligned} \quad (6)$$

where \mathbf{J}_σ is the Jacobian matrix of the softmax function σ . Thus, the attention reconstruction error is expressed as

$$\begin{aligned} \|\Delta \text{MHA}(\mathbf{X})\|_F^2 &= \|\mathbf{W}_{\text{out},h} (\Delta \mathbf{A}_h \mathbf{V}_h)^T\|_F^2 \\ &= \left\| \frac{\mathbf{W}_{\text{out},h} \mathbf{V}_h^T \mathbf{J}_\sigma^T \mathbf{K}_h}{\sqrt{d_h}} \Delta \mathbf{W}_{Q,h} \mathbf{X} \right\|_F^2. \end{aligned} \quad (7)$$

Combining this with Footnote 2 yields the following Hessian for $\mathbf{W}_{Q,h}$:

$$\begin{aligned} \mathbf{H}^{(w_{Q,h})} &= 2\mathbf{X}\mathbf{X}^T \otimes \frac{\mathbf{K}_h^T \mathbf{J}_\sigma^T \mathbf{V}_h \mathbf{W}_{\text{out},h}^T \mathbf{W}_{\text{out},h} \mathbf{V}_h^T \mathbf{J}_\sigma \mathbf{K}_h}{d_h}. \end{aligned} \quad (8)$$

Hessian for $\mathbf{W}_{K,h}$ When $\mathbf{W}_{K,h}$ is quantized, the attention weight \mathbf{A}_h changes as in the quantization of $\mathbf{W}_{Q,h}$. By following the steps for (6), \mathbf{A}_h can be approximated as

$$\Delta \mathbf{A}_h \approx \frac{\mathbf{Q}_h \Delta \mathbf{K}_h^T}{\sqrt{d_h}} \mathbf{J}_\sigma^T = \frac{\mathbf{Q}_h \Delta \mathbf{W}_{K,h} \mathbf{X} \mathbf{J}_\sigma^T}{\sqrt{d_h}}, \quad (9)$$

and thus the attention reconstruction error can be expressed as

$$\begin{aligned} \|\Delta \text{MHA}(\mathbf{X})\|_F^2 &= \|\Delta \mathbf{A}_h \mathbf{V}_h \mathbf{W}_{\text{out},h}^T\|_F^2 \\ &= \left\| \frac{\mathbf{Q}_h}{\sqrt{d_h}} \Delta \mathbf{W}_{K,h} \mathbf{X} \mathbf{J}_\sigma^T \mathbf{V}_h \mathbf{W}_{\text{out},h}^T \right\|_F^2. \end{aligned} \quad (10)$$

Thus, we obtain the following Hessian for $\mathbf{W}_{K,h}$:

$$\begin{aligned} \mathbf{H}^{(w_{K,h})} &= 2\mathbf{X} \mathbf{J}_\sigma^T \mathbf{V}_h \mathbf{W}_{\text{out},h}^T \mathbf{W}_{\text{out},h} \mathbf{V}_h^T \mathbf{J}_\sigma \mathbf{X}^T \otimes \frac{\mathbf{Q}_h^T \mathbf{Q}_h}{d_h}. \end{aligned} \quad (11)$$

Hessian for $\mathbf{W}_{V,h}$ When quantizing $\mathbf{W}_{V,h}$, only \mathbf{V}_h changes. Thus, the attention reconstruction error is expressed as

$$\begin{aligned} \|\Delta \text{MHA}(\mathbf{X})\|_F^2 &= \|\mathbf{W}_{\text{out},h} (\mathbf{A}_h \Delta \mathbf{V}_h)^T\|_F^2 \\ &= \|\mathbf{W}_{\text{out},h} \Delta \mathbf{W}_{V,h} \mathbf{X} \mathbf{A}_h^T\|_F^2, \end{aligned}$$

Algorithm 1 BOA

Input: weights $\mathbf{W} \in \mathbb{R}^{d_{\text{row}} \times d_{\text{col}}}$ and inputs \mathbf{X} of the Transformer layer

- 1: **def** BOA(\mathbf{W}, \mathbf{X})
- 2: Initialize quantized output: $\mathbf{Q} \leftarrow \mathbf{0}_{H \times d_{\text{row}}/H \times d_{\text{col}}}$
- 3: Initialize (row-wise) quantization errors: $\mathbf{E} \leftarrow \mathbf{0}_{H \times d_{\text{col}}}$
- 4: Compute attention-aware Hessians: $\mathbf{H}_h = \mathbf{H}_{\text{col},h} \otimes \mathbf{H}_{\text{row},h}$ ▷ See Table 1
- 5: Set step size (scale) \mathbf{S} : $\min_{\mathbf{S}} \text{tr}(\Delta \mathbf{W} \mathbf{H}_{\text{col},h} \Delta \mathbf{W}^T)$
- 6: Compute inverse Hessians $\mathbf{H}_{\text{col},h}^{-1}$ and $\mathbf{H}_{\text{row},h}^{-1}$
- 7: Compute $\mathbf{U}_{\text{col},h} = \text{Chol}(\mathbf{H}_{\text{col},h}^{-1})^T$ and $\mathbf{U}_{\text{row},h} = \text{Chol}(\mathbf{H}_{\text{row},h}^{-1})^T$
- 8: **for** $j = 0, \dots, d_{\text{row}}/H - 1$ **do**
- 9: Construct $\mathbf{W}^{(j)} \in \mathbb{R}^{H \times d_{\text{col}}}$ by stacking the j -th rows $[\mathbf{W}_h]_{j,:}$
- 10: Quantize $\mathbf{W}^{(j)}$: $(\mathbf{Q}_{:,j,:}, \mathbf{E}) \leftarrow \text{OPTQ}(\mathbf{W}^{(j)}, \mathbf{U}_{\text{col},h}, \mathbf{S})$ ▷ See Appendix D
- 11: Update remaining rows: $[\mathbf{W}_h]_{j,:} \leftarrow [\mathbf{W}_h]_{j,:} - \frac{[\mathbf{U}_{\text{row},h}^T]_{j,:} \cdot \mathbf{E}_{h,:} \cdot \mathbf{U}_{\text{col},h}}{[\mathbf{U}_{\text{row},h}]_{j,j}}$
- 12: **end for**

Output: quantized weights \mathbf{Q}

which yields the following Hessian for $\mathbf{W}_{V,h}$:

$$\mathbf{H}^{(\mathbf{w}_{V,h})} = 2\mathbf{X}\mathbf{A}_h^T \mathbf{A}_h \mathbf{X}^T \otimes \mathbf{W}_{\text{out},h}^T \mathbf{W}_{\text{out},h}. \quad (12)$$

Hessian for $\mathbf{W}_{\text{out},h}$ When $\mathbf{W}_{\text{out},h}$ is quantized, the attention reconstruction error is expressed as

$$\|\Delta \text{MHA}(\mathbf{X})\|_F^2 = \|\Delta \mathbf{W}_{\text{out},h} (\mathbf{A}_h \mathbf{V}_h)^T\|_F^2.$$

Thus, the corresponding Hessian is obtained as

$$\begin{aligned} \mathbf{H}^{(\mathbf{w}_{\text{out},h})} &= 2\mathbf{V}_h^T \mathbf{A}_h^T \mathbf{A}_h \mathbf{V}_h \otimes \mathbf{I} \\ &= 2\mathbf{X}_{\text{out}} \mathbf{X}_{\text{out}}^T \otimes \mathbf{I}, \end{aligned} \quad (13)$$

where $\mathbf{X}_{\text{out},h} = (\mathbf{A}_h \mathbf{V}_h)^T$ is the input to the out-projection layer.

3.2 Proposed BOA

The proposed BOA algorithm quantizes weights by repeating the quantization and weight-update steps; once BOA quantizes one weight, it updates the remaining (not-yet-quantized) weights by exploiting the Hessian-based weight-update formula in (3a) (see Algorithm 1). The key difference over OPTQ is that we exploit the attention-aware Hessians developed in Section 3.1, which facilitates the consideration of the inter-layer dependencies within the attention module.

Notably, the proposed attention-aware Hessians are significantly more complex than the conventional Hessian in (4), which may incur high computational costs. For example, computing the proposed Hessians is more expensive than computing the existing Hessian in (4). In this subsection, we

present techniques for mitigating the computational overheads incurred by the proposed attention-aware Hessians.

Hessian relaxation The largest overhead related to the computation of the proposed Hessians is the Jacobian matrix \mathbf{J}_σ in (8) and (11). For one input sequence, the shape of \mathbf{J}_σ is $H \times L \times L \times L$, which requires a large amount of memory and high computational cost.

To mitigate such computational overhead, we establish a relaxed Hessian that does not require the computation of \mathbf{J}_σ . To this end, we build an upper bound for the attention reconstruction error in (7), which will be used as its surrogate:

$$\begin{aligned} &\|\Delta \text{MHA}(\mathbf{X})\|_F^2 \\ &\leq \left\| \frac{\mathbf{W}_{\text{out},h} \mathbf{V}_h^T \mathbf{J}_\sigma}{\sqrt{d_h}} \right\|_F^2 \cdot \|\mathbf{K}_h \Delta \mathbf{W}_{Q,h} \mathbf{X}\|_F^2. \end{aligned} \quad (14)$$

Moreover, we note that the term $\|\mathbf{W}_{\text{out},h} \mathbf{V}_h^T \mathbf{J}_\sigma\|_F^2$ in (14) is constant and does not affect quantization.³ Thus, we do not need to consider this term when computing the Hessian. In short, we use the term $\|\mathbf{K}_h \Delta \mathbf{W}_{Q,h} \mathbf{X}\|_F^2$ as a surrogate of the attention reconstruction error when deriving the Hessian for $\mathbf{W}_{Q,h}$, which results in the following relaxed Hessian:

$$\mathbf{H}^{(\mathbf{w}_{Q,h})} = 2\mathbf{X}\mathbf{X}^T \otimes \mathbf{K}_h^T \mathbf{K}_h. \quad (15)$$

Similarly, we can establish a relaxed Hessian for

³The weight-update $\delta \mathbf{w}$ in (3a) is not affected by the constant multiple of $\mathbf{H}([\mathbf{c}\mathbf{U}]_{q,:}/[\mathbf{c}\mathbf{U}]_{q,q} = [\mathbf{U}]_{q,:}/[\mathbf{U}]_{q,q})$.

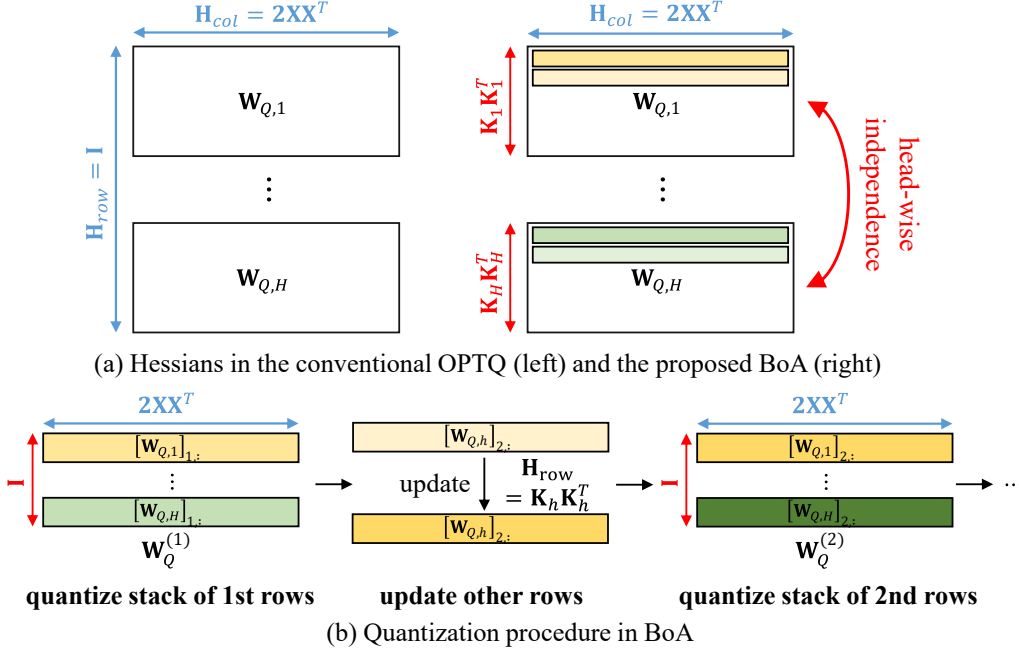


Figure 1: Illustration of the proposed BOA for the query projection \mathbf{W}_Q .

$\mathbf{W}_{K,h}$ as follows:

$$\mathbf{H}^{(\mathbf{w}_{K,h})} = 2\mathbf{X}\mathbf{X}^T \otimes \mathbf{Q}_h^T \mathbf{Q}_h. \quad (16)$$

Table 1 summarizes the proposed Hessians for each layer inside the Transformer block.

Efficient computation of inverse Hessians Owing to the size of the proposed attention-aware Hessians being $dd_h \times dd_h$, the complexity of the computation of the inverse Hessian (see (3b)) would be $\mathcal{O}(d^3 d_h^3)$ in our approach. This is considerably more expensive than the complexity $\mathcal{O}(d^3)$ in OPTQ, where the inverse of only the column-wise Hessian $\mathbf{X}\mathbf{X}^T \in \mathbb{R}^{d \times d}$ (in (4)) is needed (Frantar et al., 2023).

For the efficient computation of the inverse Hessians, we exploit the useful properties of the Kronecker product ((17a)-(17c) in Appendix A). For simplicity, let $\mathbf{H} = \mathbf{H}_{col} \otimes \mathbf{H}_{row}$ where $\mathbf{H}_{col} \in \mathbb{R}^{d \times d}$ and $\mathbf{H}_{row} \in \mathbb{R}^{d_h \times d_h}$, then we obtain

$$\mathbf{H}^{-1} = (\mathbf{H}_{col} \otimes \mathbf{H}_{row})^{-1} = \mathbf{H}_{col}^{-1} \otimes \mathbf{H}_{row}^{-1}.$$

This implies that the inverse Hessian \mathbf{H}^{-1} can be computed by computing \mathbf{H}_{col}^{-1} and \mathbf{H}_{row}^{-1} (line 6 in Algorithm 1) whose complexity is $\mathcal{O}(d^3) + \mathcal{O}(d_h^3)$ ($= \mathcal{O}(d^3)$) and not $\mathcal{O}(d^3 d_h^3)$. Similarly, we can efficiently compute the Cholesky decomposition with the same order of complexity as OPTQ. Specifically, if $\mathbf{L}_1 = \text{Chol}(\mathbf{H}_{col}^{-1})$ and $\mathbf{L}_2 = \text{Chol}(\mathbf{H}_{row}^{-1})$, \mathbf{H}^{-1} can be expressed as

$$\mathbf{H}^{-1} = \mathbf{L}_1 \mathbf{L}_1^T \otimes \mathbf{L}_2 \mathbf{L}_2^T = (\mathbf{L}_1 \otimes \mathbf{L}_2)(\mathbf{L}_1 \otimes \mathbf{L}_2)^T.$$

Subsequently, noting that the Kronecker product of lower triangular matrices is also lower triangular, we obtain

$$\begin{aligned} \text{Chol}(\mathbf{H}^{-1}) &= \mathbf{L}_1 \otimes \mathbf{L}_2 \\ &= \text{Chol}(\mathbf{H}_{col}^{-1}) \otimes \text{Chol}(\mathbf{H}_{row}^{-1}). \end{aligned}$$

Thus, we can obtain $\text{Chol}(\mathbf{H}^{-1})$ by computing $\text{Chol}(\mathbf{H}_{col}^{-1})$ and $\text{Chol}(\mathbf{H}_{row}^{-1})$ (line 7 in Algorithm 1). Consequently, the computational complexity of the Cholesky decomposition would be $\mathcal{O}(d^3)$ and not $\mathcal{O}(d^3 d_h^3)$.

Simultaneous quantization of different heads

In contrast to OPTQ wherein only column-wise Hessian is considered, the proposed BOA models both column- and row-wise Hessians (see Fig. 1(a)). Using the row-wise Hessian, we can compensate for the quantization error of a certain row by updating the other rows. However, in this case, the rows must be quantized sequentially (not simultaneously). For example, the second row can be quantized after being updated to compensate for the quantization error of the first row. This is in contrast to OPTQ, wherein the two rows are quantized simultaneously.

To accelerate the quantization process, we assume independence between different attention heads (see Fig. 1(a)). Under this assumption, the rows related to different heads are independent and can thus be quantized together. For a better understanding, we consider the query projection \mathbf{W}_Q

Table 2: INT2 quantization performance (perplexity \downarrow) of the proposed BOA and the conventional OPTQ.

(a) OPT

Dataset	Method	125M	350M	1.3B	2.7B	6.7B	13B	30B
WikiText-2	RTN	5.5e3	2.8e4	1.1e5	9.5e3	2.8e4	1.9e5	1.7e5
	OPTQ	232.8	98.65	66.76	37.44	24.74	18.97	13.12
	BoA	141.6	57.40	48.71	26.20	22.71	18.76	12.15
PTB	RTN	4.3e3	2.8e4	1.1e4	6.8e3	1.8e4	1.2e5	1.7e5
	OPTQ	384.8	135.9	112.0	64.59	42.36	26.95	20.25
	BoA	199.2	90.87	78.73	40.76	33.77	25.34	18.52
C4	RTN	3.7e3	1.6e4	7.7e3	7.7e3	1.4e4	9.7e4	5.8e4
	OPTQ	178.6	71.89	64.11	33.94	24.86	20.08	14.45
	BoA	118.1	54.07	48.92	26.57	23.03	19.22	13.84

(b) BLOOM and LLaMA

Dataset	Method	BLOOM					LLaMA	
		560M	1.1B	1.7B	3B	7.1B	13B	30B
WikiText-2	RTN	7.8e5	9.8e5	3.5e5	1.4e5	2.1e5	5.7e4	2.7e4
	OPTQ	59.23	43.93	36.48	29.25	20.20	12.67	8.844
	BoA	52.09	38.16	30.76	24.25	17.54	11.56	7.993
PTB	RTN	7.4e5	1.1e6	2.5e5	1.2e5	2.2e5	8.1e4	3.3e4
	OPTQ	142.6	176.4	95.32	67.48	43.73	20.55	14.64
	BoA	113.0	139.1	69.98	53.10	35.97	18.49	13.24
C4	RTN	1.4e6	2.1e6	2.7e5	9.2e4	1.3e5	5.9e4	2.8e4
	OPTQ	57.31	43.48	38.69	30.97	23.52	14.24	11.78
	BoA	52.12	39.03	33.71	27.26	21.22	13.34	10.53

* INT3/INT4 quantization results are provided in Appendix C.1 due to the page limitation.

as an example (see Fig. 1(b)). In the quantization step, we stack the j -th rows $[\mathbf{W}_{Q,h}]_{j,:}$, constructing $\mathbf{W}_Q^{(j)} \in \mathbb{R}^{H \times d}$ (line 9 in Algorithm 1). Because the rows of $\mathbf{W}_Q^{(j)}$ are mutually independent (*i.e.*, the row-wise Hessian is the identity), $\mathbf{W}_Q^{(j)}$ can be quantized quickly, as in OPTQ (line 10 in Algorithm 1). Following quantization, we compensate for the quantization error by updating the remaining rows. In this update step, we use the refined weight-update formula (line 11 in Algorithm 1); the detailed derivation for this is provided in Appendix B.

4 Experiments

4.1 Experimental setup

To evaluate the performance of the proposed BOA, we quantize publicly available language models including OPT (Zhang et al., 2022), BLOOM (Scao et al., 2022), and LLaMA (Touvron et al., 2023)). As in (Frantar et al., 2023; Jeon et al., 2023b; Chee et al., 2023), we quantize only weights and retain activations with full precision because activations do not pose a significant bottleneck for the inference of LLMs (Frantar et al., 2023; Kim et al.,

2023). As a calibration dataset, we use 128 random 2048 token segments from the C4 dataset (Raffel et al., 2020). Thus, we do not use any task-specific data for quantization. We evaluate the performance of the quantized models using benchmark datasets (*e.g.*, WikiText-2 (Merity et al., 2016), C4 (Raffel et al., 2020), and PTB (Marcus et al., 1993)) and zero-shot tasks. All experiments were conducted using a single NVIDIA A100 GPU (80 GB).

When determining a quantization order, the heuristic introduced by (Frantar et al., 2023) can be employed; the column/row corresponding to the largest $\text{diag}(\mathbf{H}_{\text{col}})/\text{diag}(\mathbf{H}_{\text{row}})$ (*i.e.*, the most sensitive column/row for quantization) is first quantized for better compensation. Empirically, we observed that this heuristic could occasionally enhance the performance, yet at other times, it may result in inferior performance. We conduct experiments with and without this heuristic and report the better results.

4.2 Comparison with OPTQ

We compare the proposed BOA with the conventional OPTQ (Frantar et al., 2023), which is our primary baseline. For both algorithms, we set per-channel quantization parameters (*i.e.*, scale and

Table 3: INT2 zero-shot task performance (accuracy \uparrow) of the proposed BOA and the conventional OPTQ.

Model	Size	Method	ARC-c	ARC-e	HellaSwag	MMLU	Average
OPT	1.3B	OPTQ	22.53	35.61	34.03	22.93	28.78
		BoA	22.53	38.72	36.00	23.12	30.09
	2.7B	OPTQ	24.40	38.47	37.87	23.04	30.95
		BoA	25.51	42.89	43.68	23.14	33.81
	6.7B	OPTQ	25.60	42.85	43.29	24.09	33.96
		BoA	26.62	44.91	44.52	24.33	35.10
	13B	OPTQ	26.62	44.15	50.09	24.59	36.36
		BoA	27.47	47.39	54.42	25.21	38.62
	30B	OPTQ	31.57	52.99	60.55	25.27	42.60
		BoA	31.48	53.24	62.58	26.41	43.43
LLaMA	13B	OPTQ	32.17	58.71	57.48	23.53	42.97
		BoA	33.79	59.01	59.73	23.90	44.11
	30B	OPTQ	37.12	62.84	65.09	31.16	49.05
		BoA	37.88	63.47	66.31	33.11	50.19

Table 4: INT2 performance (perplexity \downarrow) of BOA integrated with methods exploiting foldable parameters.

Folding Param. Comput. Method	Dataset	Method	OPT						
			125M	350M	1.3B	2.7B	6.7B	13B	30B
SmoothQuant	WikiText-2	OPTQ	229.4	N/A	39.88	27.31	20.03	15.32	13.55
		BoA	151.2	N/A	31.62	24.45	18.55	14.29	12.49
	PTB	OPTQ	292.3	N/A	64.17	44.75	32.01	22.03	19.26
		BoA	223.9	N/A	58.17	38.87	27.85	19.79	17.97
	C4	OPTQ	151.4	N/A	38.13	26.80	21.22	16.19	14.42
		BoA	130.4	N/A	34.20	24.95	20.92	15.33	13.90
Z-FOLD	WikiText-2	OPTQ	156.0	102.5	33.97	27.10	18.07	16.29	13.24
		BoA	107.9	54.72	29.38	23.96	17.18	15.14	12.41
	PTB	OPTQ	206.9	130.7	53.80	46.08	26.79	23.73	19.27
		BoA	166.1	82.27	49.18	39.45	24.94	22.86	18.11
	C4	OPTQ	108.8	71.37	31.67	25.98	19.79	17.21	14.13
		BoA	86.07	49.39	28.65	24.19	19.01	16.17	13.67

* SmoothQuant does not support OPT-350M where the post-LayerNorm architecture has been used.

zero-point) to minimize the layer-wise reconstruction error (line 5 in Algorithm 1). We note that in OPTQ, the Min-Max-based quantization parameters have been used (Frantar et al., 2023); however, this results in significantly worse quantization performance (Chee et al., 2023; Jeon et al., 2023b). To compare the pure performance of the proposed BOA and OPTQ, we do not use foldable parameters in this experiment. The results of using the foldable parameters are presented in Section 4.3.

First, we compare the perplexity (PPL) performance of BOA and OPTQ (Table 2). The performance of the rounding-to-nearest (RTN) method (which naively assigns the nearest quantized value) is also included for comparison, as in (Frantar et al., 2023). While RTN collapses completely for low bit-widths, BOA and OPTQ exhibit reasonable PPL, even for INT2 quantization. This is because BOA

and OPTQ minimize the task loss degradation, not the weight quantization error $\Delta\mathbf{W}$, by exploiting the Hessian. Moreover, our method outperforms OPTQ for all models. In particular, the performance gap is significant for low bit-width (*i.e.*, INT2) and small-sized models suited for resource-limited devices (*e.g.*, mobile devices).

To compare the zero-shot performance of the proposed BOA and OPTQ, we measure the accuracy of the quantized models for several tasks and then average the results. We note that the zero-shot setting is maintained in our experiments because we do not use task-specific data for quantization. As shown in Table 3, the proposed BOA outperforms OPTQ for all models. The key factor leading to such an outstanding performance is that we consider inter-layer dependencies within the attention module by targeting attention-wise reconstruction.

Table 5: INT2 zero-shot performance (accuracy \uparrow) of BOA integrated with methods exploiting foldable parameters.

Folding Param. Comput. Method	OPT	Method	Tasks				Average
			ARC-c	ARC-e	HellaSwag	MMLU	
SmoothQuant	1.3B	OPTQ	23.38	40.15	37.47	23.00	31.00
		BoA	22.18	42.00	37.48	23.10	31.19
	2.7B	OPTQ	25.85	42.72	42.46	23.10	33.53
		BoA	27.73	44.70	44.24	22.95	34.91
	6.7B	OPTQ	25.68	46.25	45.24	23.40	35.14
		BoA	27.56	48.15	46.20	23.90	36.45
	13B	OPTQ	29.52	52.53	56.63	24.90	40.90
		BoA	31.57	53.66	58.69	25.35	42.32
	30B	OPTQ	29.18	54.46	60.04	24.54	42.06
		BoA	31.57	55.93	62.18	25.54	43.81
Z-FOLD	1.3B	OPTQ	23.89	42.05	40.45	23.07	32.37
		BoA	24.74	43.98	40.31	23.45	33.12
	2.7B	OPTQ	25.00	41.46	43.13	23.16	33.19
		BoA	26.37	43.06	45.18	23.50	34.53
	6.7B	OPTQ	30.46	48.78	52.46	25.64	39.34
		BoA	28.58	49.75	55.45	26.67	40.11
	13B	OPTQ	28.58	48.78	55.38	24.75	39.37
		BoA	28.84	49.87	58.32	24.60	40.41
	30B	OPTQ	31.83	53.70	61.34	24.96	42.96
		BoA	30.12	57.53	63.63	24.85	44.03

This is in contrast to OPTQ, where layers are assumed to be independent.

4.3 Integration with Existing Works

As mentioned in Section 2.1, recent studies have used foldable parameters for more precise quantization (Xiao et al., 2023; Jeon et al., 2023b; Lin et al., 2024; Shao et al., 2023; Ma et al., 2024). Because these approaches are orthogonal to ours, we can further enhance the quantization performance by integrating them with the proposed BOA. Among the various algorithms, we employ SmoothQuant (Xiao et al., 2023) and Z-FOLD (Jeon et al., 2023b) in our integration because they efficiently compute foldable parameters without time-consuming gradient-based optimization.⁴

Table 4 summarizes the PPL performance of the proposed BOA combined with SmoothQuant and Z-FOLD. For comparison, we also summarize the integration results for the conventional OPTQ. Overall, the performances of both BOA and OPTQ improve when using the folding parameters. Moreover, the performance gap between the proposed BOA and OPTQ remains significant, even when the folding parameters are used. In particular, when

combined with Z-FOLD, BOA outperforms other algorithms that learn attention-aware folding parameters via backpropagation by a significant margin (further details in Appendix C.3).

A similar behavior is observed in the zero-shot results (Table 5); the performance is boosted by leveraging the folding parameters, and BOA outperforms OPTQ for all models regardless of the folding parameter computation method.

5 Conclusion

In this paper, we proposed a novel PTQ algorithm called BOA. To consider the inter-layer dependencies within the attention module while circumventing time-consuming gradient-based optimization, we approximated the Hessian matrices by exploiting the attention reconstruction error. Furthermore, to mitigate the computational overhead incurred by the proposed attention-aware Hessians, we incorporated several techniques, such as Hessian relaxation, efficient computation of inverse Hessians, and head-wise simultaneous quantization. Finally, through extensive experiments, we demonstrated the efficacy of the proposed BOA algorithm.

⁴SmoothQuant and Z-FOLD determine foldable parameters using a pre-defined heuristic rule and alternating least squares, respectively.

6 Limitations

Recall that we used the attention reconstruction error to approximate the Hessian matrix. If the reconstruction error for the entire Transformer block is used, then the dependencies between more layers, including fully-connected layers, can be considered, resulting in further enhancement at the expense of higher computational cost. Furthermore, we did not consider activation quantization in this study because activations do not pose a significant bottleneck, and the inference of LLMs can be sufficiently accelerated by reducing memory movement via weight quantization (Frantar et al., 2023; Kim et al., 2023). For the scenarios wherein the activation needs to be quantized, orthogonal techniques (Xiao et al., 2023; Yao et al., 2022) can be combined with the proposed BOA, which will be considered in future studies.

References

- Jerry Chee, Yaohui Cai, Volodymyr Kuleshov, and Christopher De Sa. 2023. QuIP: 2-bit quantization of large language models with guarantees. In *Thirty-seventh Conference on Neural Information Processing Systems*.
- Elias Frantar and Dan Alistarh. 2022. Optimal brain compression: A framework for accurate post-training quantization and pruning. *Advances in Neural Information Processing Systems*, 35:4475–4488.
- Elias Frantar, Saleh Ashkboos, Torsten Hoefler, and Dan Alistarh. 2023. OPTQ: Accurate quantization for generative pre-trained Transformers. In *The Eleventh International Conference on Learning Representations*.
- Itay Hubara, Yury Nahshan, Yair Hanani, Ron Banner, and Daniel Soudry. 2021. Accurate post training quantization with small calibration sets. In *International Conference on Machine Learning*, pages 4466–4475. PMLR.
- Yongkweon Jeon, Chungman Lee, Eulrang Cho, and Yeonju Ro. 2022. Mr. BiQ: Post-training non-uniform quantization based on minimizing the reconstruction error. In *Proceedings of the IEEE/CVF Conference on Computer Vision and Pattern Recognition*, pages 12329–12338.
- Yongkweon Jeon, Chungman Lee, and Ho-young Kim. 2023a. Genie: show me the data for quantization. In *Proceedings of the IEEE/CVF Conference on Computer Vision and Pattern Recognition*, pages 12064–12073.
- Yongkweon Jeon, Chungman Lee, Kyungphil Park, and Ho-young Kim. 2023b. A frustratingly easy post-training quantization scheme for LLMs. In *Proceedings of the 2023 Conference on Empirical Methods in Natural Language Processing*, pages 14446–14461.
- Sehoon Kim, Coleman Hooper, Amir Gholami, Zhen Dong, Xiuyu Li, Sheng Shen, Michael W Mahoney, and Kurt Keutzer. 2023. SqueezeLLM: Dense-and-sparse quantization. *arXiv:2306.07629*.
- Yann LeCun, John S Denker, Sara A Solla, Richard E Howard, and Lawrence D Jackel. 1989. Optimal brain damage. In *Advances in Neural Information Processing Systems (NIPS)*, volume 2, pages 598–605.
- Changhun Lee, Jungyu Jin, Taesu Kim, Hyungjun Kim, and Eunhyeok Park. 2023. OWQ: Lessons learned from activation outliers for weight quantization in large language models. *arXiv preprint arXiv:2306.02272*.
- Yuhang Li, Ruihao Gong, Xu Tan, Yang Yang, Peng Hu, Qi Zhang, Fengwei Yu, Wei Wang, and Shi Gu. 2021. BRECC: Pushing the limit of post-training quantization by block reconstruction. In *International Conference on Learning Representations (ICLR)*.
- Ji Lin, Jiaming Tang, Haotian Tang, Shang Yang, Weiming Chen, Wei-Chen Wang, Guangxuan Xiao, Xingyu Dang, Chuang Gan, and Song Han. 2024. AWQ: Activation-aware weight quantization for LLM compression and acceleration. In *MLSys*.
- Yuxiao Ma, Huixia Li, Xiawu Zheng, Feng Ling, Xuefeng Xiao, Rui Wang, Shilei Wen, Fei Chao, and Rongrong Ji. 2024. AffineQuant: Affine transformation quantization for large language models. *arXiv:2403.12544*.
- Mitchell Marcus, Beatrice Santorini, and Mary Ann Marcinkiewicz. 1993. Building a large annotated corpus of english: The penn treebank.
- Stephen Merity, Caiming Xiong, James Bradbury, and Richard Socher. 2016. Pointer sentinel mixture models. *arXiv:1609.07843*.
- Markus Nagel, Rana Ali Amjad, Mart Van Baalen, Christos Louizos, and Tijmen Blankevoort. 2020. Up or down? Adaptive rounding for post-training quantization. In *International Conference on Machine Learning (ICML)*, pages 7197–7206.
- Colin Raffel, Noam Shazeer, Adam Roberts, Katherine Lee, Sharan Narang, Michael Matena, Yanqi Zhou, Wei Li, and Peter J Liu. 2020. Exploring the limits of transfer learning with a unified text-to-text transformer. *Journal of Machine Learning Research*, 21(1):5485–5551.
- Teven Le Scao, Angela Fan, Christopher Akiki, Elie Pavlick, Suzana Ilić, Daniel Hesslow, Roman Castagné, Alexandra Sasha Luccioni, François Yvon, Matthias Gallé, et al. 2022. BLOOM: A 176B-parameter open-access multilingual language model. *arXiv:2211.05100*.

Wenqi Shao, Mengzhao Chen, Zhaoyang Zhang, Peng Xu, Lirui Zhao, Zhiqian Li, Kaipeng Zhang, Peng Gao, Yu Qiao, and Ping Luo. 2023. OmniQuant: Omnidirectionally calibrated quantization for large language models. *arXiv:2308.13137*.

Hugo Touvron, Thibaut Lavril, Gautier Izacard, Xavier Martinet, Marie-Anne Lachaux, Timothée Lacroix, Baptiste Rozière, Naman Goyal, Eric Hambro, Faisal Azhar, et al. 2023. LLaMA: Open and efficient foundation language models. *arXiv:2302.13971*.

Guangxuan Xiao, Ji Lin, Mickael Seznec, Hao Wu, Julien Demouth, and Song Han. 2023. SmoothQuant: Accurate and efficient post-training quantization for large language models. In *International Conference on Machine Learning*, pages 38087–38099. PMLR.

Zhewei Yao, Reza Yazdani Aminabadi, Minjia Zhang, Xiaoxia Wu, Conglong Li, and Yuxiong He. 2022. ZeroQuant: Efficient and affordable post-training quantization for large-scale Transformers. *Advances in Neural Information Processing Systems*, 35:27168–27183.

Susan Zhang, Stephen Roller, Naman Goyal, Mikel Artetxe, Moya Chen, Shuohui Chen, Christopher Dewan, Mona Diab, Xian Li, Xi Victoria Lin, et al. 2022. OPT: Open pre-trained Transformer language models. *arXiv:2205.01068*.

Appendices

A Proof of Footnote 2

In our proof, we use the following useful properties of the Kronecker product:

$$\text{vec}(\mathbf{M}_1 \mathbf{M}_2 \mathbf{M}_3) = (\mathbf{M}_3^T \otimes \mathbf{M}_1) \text{vec}(\mathbf{M}_2), \quad (17a)$$

$$(\mathbf{M}_1 \otimes \mathbf{M}_2)^T = \mathbf{M}_1^T \otimes \mathbf{M}_2^T, \quad (17b)$$

$$(\mathbf{M}_1 \otimes \mathbf{M}_2) (\mathbf{M}_3 \otimes \mathbf{M}_4) = \mathbf{M}_1 \mathbf{M}_3 \otimes \mathbf{M}_2 \mathbf{M}_4, \quad (17c)$$

where $\text{vec}(\cdot)$ denotes the vectorization operation.

Using (17a), we have

$$\|\mathbf{M}_1 \Delta \mathbf{W} \mathbf{M}_2\|_F^2 = \|(\mathbf{M}_2^T \otimes \mathbf{M}_1) \Delta \mathbf{w}\|_2^2 = \Delta \mathbf{w}^T (\mathbf{M}_2^T \otimes \mathbf{M}_1)^T (\mathbf{M}_2^T \otimes \mathbf{M}_1) \Delta \mathbf{w},$$

where $\Delta \mathbf{w} = \text{vec}(\Delta \mathbf{W})$. In addition, by (17b) and (17c), we have

$$\begin{aligned} \Delta \mathbf{w}^T (\mathbf{M}_2^T \otimes \mathbf{M}_1)^T (\mathbf{M}_2^T \otimes \mathbf{M}_1) \Delta \mathbf{w} &= \Delta \mathbf{w}^T (\mathbf{M}_2 \otimes \mathbf{M}_1^T) (\mathbf{M}_2^T \otimes \mathbf{M}_1) \Delta \mathbf{w} \\ &= \Delta \mathbf{w}^T (\mathbf{M}_2 \mathbf{M}_2^T \otimes \mathbf{M}_1^T \mathbf{M}_1) \Delta \mathbf{w}. \end{aligned}$$

Finally, by exploiting the fact that $\frac{\partial^2 \mathbf{x}^T \mathbf{A} \mathbf{x}}{\partial \mathbf{x}^2} = \mathbf{A} + \mathbf{A}^T$, we obtain

$$\begin{aligned} \frac{\partial^2 \|\mathbf{M}_1 \Delta \mathbf{W} \mathbf{M}_2\|_F^2}{\partial \Delta \mathbf{w}^2} &= \mathbf{M}_2 \mathbf{M}_2^T \otimes \mathbf{M}_1^T \mathbf{M}_1 + (\mathbf{M}_2 \mathbf{M}_2^T \otimes \mathbf{M}_1^T \mathbf{M}_1)^T \\ &\stackrel{(a)}{=} \mathbf{M}_2 \mathbf{M}_2^T \otimes \mathbf{M}_1^T \mathbf{M}_1 + (\mathbf{M}_2 \mathbf{M}_2^T)^T \otimes (\mathbf{M}_1^T \mathbf{M}_1)^T \\ &= 2\mathbf{M}_2 \mathbf{M}_2^T \otimes \mathbf{M}_1^T \mathbf{M}_1, \end{aligned}$$

where (a) follows from (17b). This completes the proof.

B Refined Weight-update Formula

We recall that the Hessian-based weight-update formula is given by (Frantar and Alistarh, 2022; Frantar et al., 2023)

$$\delta \mathbf{w} = -\frac{w_q - \mathcal{Q}(w_q)}{[\mathbf{U}]_{q,q}} [\mathbf{U}]_{q,:}, \text{ where } \mathbf{U} = \text{Chol}(\mathbf{H}^{-1})^T.$$

For the proposed attention-aware Hessians in Table 1, we have

$$\mathbf{U}_h = \mathbf{U}_{\text{col},h} \otimes \mathbf{U}_{\text{row},h},$$

where $\mathbf{U}_{\text{col},h} = \text{Chol}(\mathbf{H}_{\text{col},h}^{-1})^T$ and $\mathbf{U}_{\text{row},h} = \text{Chol}(\mathbf{H}_{\text{row},h}^{-1})^T$ (see Section 3.2). Therefore, the weight-update formula can be recast as

$$\delta \mathbf{w}_h = -\frac{w_q - \mathcal{Q}(w_q)}{[\mathbf{U}_{\text{col},h} \otimes \mathbf{U}_{\text{row},h}]_{q,q}} [\mathbf{U}_{\text{col},h} \otimes \mathbf{U}_{\text{row},h}]_{q,:}.$$

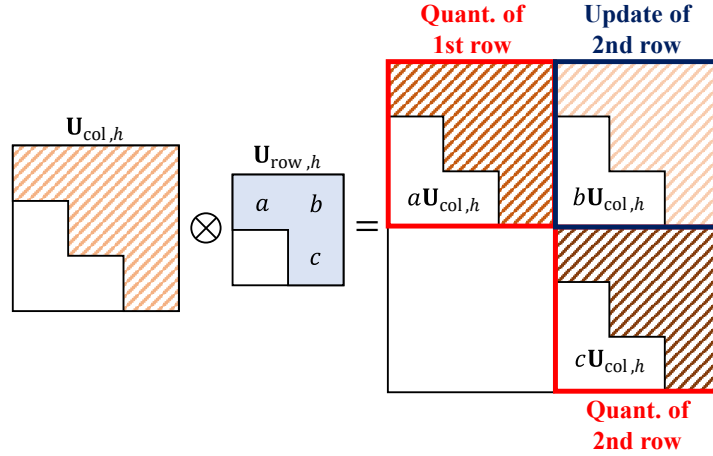


Figure 2: Illustration of the Hessian information when $d_{\text{row}} = 2$ and $d_{\text{col}} = 3$

For simplicity, suppose we quantize the first (0-th) row. When the weight $[\mathbf{W}_h]_{0,j} (= [\mathbf{W}^{(0)}]_{h,j})$ in the j -th column is quantized, the weight-update of the i -th row is simplified as (see Fig. 2 for the ease of understanding)

$$\begin{aligned} [\delta \mathbf{W}_h]_{i,:} &= -\frac{[\mathbf{W}_h]_{0,j} - \mathcal{Q}([\mathbf{W}_h]_{0,j})}{[\mathbf{U}_{\text{row},h}]_{0,0} [\mathbf{U}_{\text{col},h}]_{j,j}} [\mathbf{U}_{\text{row},h}]_{0,i} [\mathbf{U}_{\text{col},h}]_{j,:} \\ &= -\frac{[\mathbf{W}_h]_{0,j} - \mathcal{Q}([\mathbf{W}_h]_{0,j})}{[\mathbf{U}_{\text{col},h}]_{j,j}} \cdot \frac{[\mathbf{U}_{\text{row},h}]_{0,i} [\mathbf{U}_{\text{col},h}]_{j,:}}{[\mathbf{U}_{\text{row},h}]_{0,0}} \end{aligned}$$

Thus, after the quantization of all weights in the first row, the total amount of the weight-update for the i -th row can be expressed as

$$\begin{aligned} [\delta \mathbf{W}_{h,\text{total}}]_{i,:} &= -\sum_{j=0}^{d_{\text{col}}-1} \frac{[\mathbf{W}_h]_{0,j} - \mathcal{Q}([\mathbf{W}_h]_{0,j})}{[\mathbf{U}_{\text{col},h}]_{j,j}} \cdot \frac{[\mathbf{U}_{\text{row},h}]_{0,i} [\mathbf{U}_{\text{col},h}]_{j,:}}{[\mathbf{U}_{\text{row},h}]_{0,0}} \\ &= -\frac{[\mathbf{U}_{\text{row},h}]_{0,i}}{[\mathbf{U}_{\text{row},h}]_{0,0}} \sum_{j=0}^{d_{\text{col}}-1} \frac{[\mathbf{W}_h]_{0,j} - \mathcal{Q}([\mathbf{W}_h]_{0,j})}{[\mathbf{U}_{\text{col},h}]_{j,j}} \cdot [\mathbf{U}_{\text{col},h}]_{j,:}. \end{aligned}$$

Furthermore, by noting that (see line 8 in Algorithm 2)

$$[\mathbf{E}_{\text{OPTQ}}]_{h,j} = \frac{[\mathbf{W}_h]_{0,j} - \mathcal{Q}([\mathbf{W}_h]_{0,j})}{[\mathbf{U}_{\text{col},h}]_{j,j}},$$

we obtain

$$[\delta \mathbf{W}_{h,\text{total}}]_{i,:} = -\frac{[\mathbf{U}_{\text{row},h}]_{0,i}}{[\mathbf{U}_{\text{row},h}]_{0,0}} \sum_{j=0}^{d_{\text{col}}-1} [\mathbf{E}_{\text{OPTQ}}]_{h,j} \cdot [\mathbf{U}_{\text{col},h}]_{j,:} = -\frac{[\mathbf{U}_{\text{row},h}]_{0,i}}{[\mathbf{U}_{\text{row},h}]_{0,0}} [\mathbf{E}_{\text{OPTQ}}]_{h,:} \mathbf{U}_{\text{col},h}.$$

As a result, the weight-update matrix to compensate for the quantization error of the first row is given by

$$[\delta \mathbf{W}_{h,\text{total}}]_{0,:} = -\frac{[\mathbf{U}_{\text{row},h}^T]_{0,0} [\mathbf{E}_{\text{OPTQ}}]_{h,:} \mathbf{U}_{\text{col},h}}{[\mathbf{U}_{\text{row},h}]_{0,0}}. \quad (18)$$

By taking similar steps as above, we can easily generalize (18) for the j -th row as follows:

$$[\delta \mathbf{W}_{h,\text{total}}]_{j,:} = -\frac{[\mathbf{U}_{\text{row},h}^T]_{j,j} [\mathbf{E}_{\text{OPTQ}}]_{h,:} \mathbf{U}_{\text{col},h}}{[\mathbf{U}_{\text{row},h}]_{j,j}}. \quad (19)$$

C Additional Experimental Results

In this appendix, we provide experimental results omitted in the main text due to the page limitation.

C.1 Comparison with OPTQ

Table 6 and Table 7 summarize the INT3/INT4 quantization performances (perplexity) of the proposed BOA and the conventional OPTQ on various sizes of OPT, BLOOM, and LLaMA models. As evident from Table 2, Table 6, and Table 7, BOA uniformly outperforms OPTQ, and the performance gap is significant for low bit-width (*i.e.*, INT2) and small-sized models suited for resource-limited devices (*e.g.*, mobile devices).

Table 6: Quantization performance (perplexity \downarrow) of the proposed BOA and the conventional OPTQ on OPT.

(a) WikiText-2								
Precision	Method	125M	350M	1.3B	2.7B	6.7B	13B	30B
FP16	Baseline	27.65	22.00	14.63	12.47	10.86	10.13	9.56
INT4	RTN	37.28	25.94	48.20	16.92	12.10	11.32	10.98
	OPTQ	30.24	23.50	14.84	12.53	11.09	10.26	9.608
	BoA	28.93	22.90	14.72	12.44	10.88	10.16	9.571
INT3	RTN	1.3e3	64.57	1.3e4	1.6e4	5.8e3	3.4e3	1.6e3
	OPTQ	38.74	26.31	16.70	14.01	11.91	10.85	9.911
	BoA	33.68	24.69	15.93	13.43	11.53	10.58	9.826

(b) PTB								
Precision	Method	125M	350M	1.3B	2.7B	6.7B	13B	30B
FP16	Baseline	38.99	31.08	20.29	17.97	15.77	14.52	14.04
INT4	RTN	53.88	36.79	75.37	32.41	18.86	16.41	15.44
	OPTQ	44.31	33.41	21.23	18.70	16.09	14.69	14.18
	BoA	41.50	32.58	21.02	18.42	15.90	14.63	14.18
INT3	RTN	1.4e3	87.21	1.5e4	1.4e4	5.3e3	2.2e3	1.5e3
	OPTQ	57.62	39.35	24.77	21.53	17.56	15.68	14.56
	BoA	48.50	36.83	23.53	20.33	16.86	15.21	14.50

(c) C4								
Precision	Method	125M	350M	1.3B	2.7B	6.7B	13B	30B
FP16	Baseline	26.56	22.59	16.07	14.34	12.71	12.06	11.44
INT4	RTN	33.88	26.21	27.50	18.83	14.37	13.32	13.55
	OPTQ	28.53	23.73	16.51	14.72	12.88	12.16	11.50
	BoA	27.56	23.20	16.39	14.61	12.84	12.16	11.51
INT3	RTN	834.4	55.15	6.6e3	1.2e4	5.0e3	2.8e3	1.8e3
	OPTQ	33.90	26.68	18.18	16.10	13.60	12.62	11.76
	BoA	31.12	25.39	17.74	15.83	13.34	12.52	11.75

Table 7: Quantization performance (perplexity \downarrow) of the proposed BoA and OPTQ on BLOOM and LLaMA.

(a) WikiText-2								
Precision	Method	BLOOM					LLaMA	
		560M	1.1B	1.7B	3B	7.1B	13B	30B
FP16	Baseline	22.42	17.69	15.39	13.48	11.37	5.091	4.101
INT4	RTN	25.82	19.98	16.96	14.75	12.09	5.525	4.536
	OPTQ	23.44	18.54	15.90	13.90	11.63	5.262	4.285
	BoA	23.28	18.32	15.81	13.84	11.58	5.243	4.262
INT3	RTN	56.74	49.85	63.37	39.07	17.35	11.78	14.87
	OPTQ	26.63	20.80	17.71	15.39	12.42	5.721	4.848
	BoA	25.90	20.28	17.12	14.91	12.19	5.676	4.725

(b) PTB								
Precision	Method	BLOOM					LLaMA	
		560M	1.1B	1.7B	3B	7.1B	13B	30B
FP16	Baseline	43.69	57.96	30.00	25.34	20.83	9.081	8.159
INT4	RTN	50.96	66.79	33.52	27.65	22.40	9.775	8.653
	OPTQ	45.33	61.94	31.37	26.39	21.40	9.306	8.344
	BoA	44.92	61.40	30.67	26.23	21.34	9.255	8.304
INT3	RTN	124.8	184.0	105.5	66.24	34.94	28.94	28.79
	OPTQ	52.39	70.68	35.06	28.99	23.46	9.928	8.925
	BoA	50.71	67.77	33.92	28.67	22.86	9.857	8.737

(c) C4								
Precision	Method	BLOOM					LLaMA	
		560M	1.1B	1.7B	3B	7.1B	13B	30B
FP16	Baseline	26.60	22.05	19.49	17.49	15.20	6.798	6.131
INT4	RTN	29.80	24.42	21.24	18.75	16.05	7.232	6.537
	OPTQ	27.39	22.69	20.03	17.89	15.44	6.973	6.294
	BoA	27.23	22.54	19.90	17.82	15.42	6.958	6.267
INT3	RTN	66.99	60.41	113.6	79.84	22.54	14.46	30.04
	OPTQ	29.89	24.48	21.44	19.07	16.24	7.504	6.840
	BoA	29.39	24.17	21.02	18.74	16.09	7.454	6.718

C.2 Integration with SmoothQuant and Z-FOLD

Table 4 and Table 8 summarize the PPL performances of the proposed BOA combined with SmoothQuant and Z-FOLD. For comparison, we also summarize the integration results for the conventional OPTQ. Overall, we observe that the performances of both BOA and OPTQ improve when leveraging the folding parameters. We also observe that even when the folding parameters are used, the performance gap between the proposed BOA and OPTQ is still significant, especially for INT2 quantization and small-sized models suited for resource-limited devices. In particular, when combined with Z-FOLD, BOA outperforms other algorithms that learn attention-aware folding parameters via backpropagation (*e.g.*, OmniQuant (Shao et al., 2023), AffineQuant (Ma et al., 2024)) by a large margin (see Table 9 in Appendix C.3).

Table 8: INT3 performance (perplexity ↓) of BOA integrated with methods exploiting foldable parameters.

Folding Param. Comput. Method	Dataset	Method	OPT						
			125M	350M	1.3B	2.7B	6.7B	13B	30B
SmoothQuant	WikiText-2	OPTQ	39.56	N/A	16.32	13.55	11.90	10.68	9.857
		BoA	34.58	N/A	15.83	13.33	11.58	10.38	9.846
	PTB	OPTQ	58.00	N/A	24.00	20.36	17.18	15.45	14.46
		BoA	51.44	N/A	22.78	19.83	16.74	15.18	14.40
	C4	OPTQ	34.98	N/A	17.78	15.68	13.50	12.55	11.74
		BoA	31.52	N/A	17.43	15.48	13.35	12.48	11.73
Z-FOLD	WikiText-2	OPTQ	39.59	25.97	16.10	13.54	11.65	10.64	9.887
		BoA	33.31	24.22	15.91	13.33	11.28	10.53	9.814
	PTB	OPTQ	53.08	39.23	22.73	20.18	16.64	15.22	14.57
		BoA	46.59	36.80	22.29	19.54	16.44	15.16	14.53
	C4	OPTQ	33.67	26.45	17.33	15.50	13.28	12.46	11.73
		BoA	30.00	25.04	17.13	15.32	13.20	12.41	11.71

* SmoothQuant does not support OPT-350M where the post-LayerNorm architecture has been used.

C.3 Comparison with OmniQuant and AffineQuant

We compare the proposed BOA with OmniQuant (Shao et al., 2023) and AffineQuant (Ma et al., 2024), recently proposed algorithms that learn attention-aware folding parameters via backpropagation (see Table 9). As evident, BOA itself outperforms conventional attention-aware quantization schemes in almost all cases, even though BOA does not rely on time-consuming backpropagation and thus enables fast quantization (see Table 9(c)). While OmniQuant shows comparable speed by reducing the number of learnable parameters (Shao et al., 2023), it sometimes diverges or collapses (*i.e.*, PPL is larger than 10^3) for INT2 quantization.⁵ Furthermore, when combined with SmoothQuant or Z-FOLD (that finds folding parameters without backpropagation), the performance gap between BOA and OmniQuant/AffineQuant is significant, which demonstrates the efficacy of the proposed method.

Table 9: Performance (perplexity ↓) of BOA and conventional backpropagation-based attention-aware methods.

(a) INT2 quantization

Dataset	Method	125M	1.3B	2.7B	6.7B	13B	30B
WikiText-2	OmniQuant (Shao et al., 2023)	NaN	NaN	NaN	2.3e4	4.5e5	3.8e5
	AffineQuant (Ma et al., 2024)	174.5	NaN	42.26	26.25	38.89	5.6e5
	BOA	141.6	48.71	26.20	22.71	18.76	12.15
	BOA + SmoothQuant	151.2	31.62	24.45	18.55	14.29	12.49
	BOA + Z-FOLD	107.9	29.38	23.96	17.18	15.14	12.41
PTB	OmniQuant (Shao et al., 2023)	NaN	NaN	NaN	5.0e4	3.7e5	2.9e5
	AffineQuant (Ma et al., 2024)	254.2	NaN	55.58	37.36	50.10	3.1e5
	BOA	199.2	78.73	40.76	33.77	25.34	18.52
	BOA + SmoothQuant	223.9	58.17	38.87	27.85	19.79	17.97
	BOA + Z-FOLD	166.1	49.18	39.45	24.94	22.86	18.11
C4	OmniQuant (Shao et al., 2023)	NaN	NaN	NaN	3.0e4	2.0e5	2.1e5
	AffineQuant (Ma et al., 2024)	107.0	NaN	34.45	25.11	31.50	3.3e5
	BOA	118.1	48.92	26.57	23.03	19.22	13.84
	BOA + SmoothQuant	130.4	34.20	24.95	20.92	15.33	13.90
	BOA + Z-FOLD	86.07	28.65	24.19	19.01	16.17	13.67

* ‘NaN’ means that loss diverges in the quantization process.

(b) INT3 quantization

Dataset	Method	125M	1.3B	2.7B	6.7B	13B	30B
WikiText-2	OmniQuant (Shao et al., 2023)	41.59	18.23	15.11	12.86	12.49	11.26
	AffineQuant (Ma et al., 2024)	37.75	17.12	14.32	12.42	11.93	10.72
	BOA	33.68	15.93	13.43	11.53	10.58	9.826
	BOA + SmoothQuant	34.58	15.83	13.33	11.58	10.38	9.846
	BOA + Z-FOLD	33.31	15.91	13.33	11.28	10.53	9.814
PTB	OmniQuant (Shao et al., 2023)	59.51	26.08	22.68	18.31	17.76	16.02
	AffineQuant (Ma et al., 2024)	53.02	24.47	21.18	17.27	17.27	15.31
	BOA	48.50	23.53	20.33	16.86	15.21	14.50
	BOA + SmoothQuant	51.44	22.78	19.83	16.74	15.18	14.40
	BOA + Z-FOLD	46.59	22.29	19.54	16.44	15.16	14.53
C4	OmniQuant (Shao et al., 2023)	35.73	19.10	16.80	14.40	13.48	12.44
	AffineQuant (Ma et al., 2024)	33.37	18.56	16.15	13.91	13.31	12.14
	BOA	31.12	17.74	15.83	13.34	12.52	11.75
	BOA + SmoothQuant	31.52	17.43	15.48	13.35	12.48	11.73
	BOA + Z-FOLD	30.00	17.13	15.32	13.20	12.41	11.71

(c) INT2 quantization processing time

Method	125M	1.3B	2.7B	6.7B	13B	30B
OmniQuant (Shao et al., 2023)	16.20 min	61.20 min	1.627 hr	2.933 hr	5.309 hr	11.57 hr
AffineQuant (Ma et al., 2024)	28.33 min	154.2 min	4.597 hr	9.854 hr	18.41 hr	44.25 hr
BOA	5.099 min	31.64 min	1.101 hr	2.830 hr	4.964 hr	10.55 hr

⁵In OmniQuant and AffineQuant, group-wise quantization parameters have been used to supplement the INT2 quantization performance (Shao et al., 2023; Ma et al., 2024), which incurs additional memory and computational costs.

C.4 Results for Different Calibration Datasets

When constructing a calibration dataset, we randomly sample 128 sequences from the C4 dataset (see Section 4.1). By changing the seed for the sampling, we can obtain different calibration datasets, which leads to different quantization results.⁶ In this appendix, we report the corresponding results and overall statistics. Due to the limited computational resources, we conducted this experiment only for our main comparison (*i.e.*, the performances of the proposed BOA and the conventional OPTQ).

Table 10: Performance (perplexity \downarrow) of the proposed BOA and the conventional OPTQ for different seeds.

(a) INT2 Quantization

Dataset	Seed	Method	125M	350M	1.3B	2.7B	6.7B	13B	30B
WikiText-2	0	OPTQ	232.8	98.65	66.76	37.44	24.74	18.97	13.12
		BoA	141.6	57.40	48.71	26.20	22.71	18.76	12.15
	10	OPTQ	276.2	103.4	66.30	36.74	24.64	20.05	13.34
		BoA	147.4	57.54	47.23	25.95	23.11	18.52	12.17
	20	OPTQ	243.9	98.70	65.09	36.33	24.94	19.78	13.17
		BoA	139.4	61.30	45.11	27.00	24.06	17.82	12.33
	50	OPTQ	269.9	90.11	64.88	33.84	24.54	19.47	13.41
		BoA	160.7	59.47	44.13	26.75	23.09	18.70	12.15
	100	OPTQ	228.3	98.94	71.51	36.72	25.55	19.39	13.18
		BoA	147.8	60.56	47.43	26.85	23.61	18.49	12.17
	Mean \pm Stdev	OPTQ	250.2 \pm 22	97.96 \pm 4.8	66.91 \pm 2.7	36.21 \pm 1.4	24.88 \pm 0.40	19.53 \pm 0.41	13.24 \pm 0.12
		BoA	147.4 \pm 8.3	59.25 \pm 1.8	46.52 \pm 1.9	26.55 \pm 0.45	23.32 \pm 0.53	18.46 \pm 0.38	12.19 \pm 0.077
PTB	0	OPTQ	384.8	135.9	112.0	64.59	42.36	26.95	20.25
		BoA	199.2	90.87	78.73	40.76	33.77	25.34	18.52
	10	OPTQ	324.1	161.6	112.7	62.42	38.91	27.92	19.80
		BoA	185.4	86.16	76.02	39.73	33.79	23.55	18.08
	20	OPTQ	350.4	127.9	111.6	62.64	39.84	27.80	20.57
		BoA	188.7	86.60	79.31	41.69	34.89	24.59	18.06
	50	OPTQ	433.8	134.2	122.1	59.46	43.05	27.64	20.43
		BoA	206.8	84.94	87.29	41.91	36.36	24.56	18.27
	100	OPTQ	479.2	142.9	125.8	59.49	38.26	27.56	20.02
		BoA	164.8	87.16	77.32	41.67	35.19	24.56	17.98
	Mean \pm Stdev	OPTQ	394.5 \pm 63	140.5 \pm 13	116.8 \pm 6.6	61.72 \pm 2.2	40.48 \pm 2.1	27.57 \pm 0.38	20.21 \pm 0.31
		BoA	189.0 \pm 16	87.15 \pm 2.2	79.73 \pm 4.4	41.15 \pm 0.91	34.80 \pm 1.1	24.52 \pm 0.64	18.18 \pm 0.22
C4	0	OPTQ	178.6	71.89	64.11	33.94	24.86	20.08	14.45
		BoA	118.1	54.07	48.92	26.57	23.03	19.22	13.84
	10	OPTQ	189.7	72.94	64.19	33.27	24.40	20.40	14.44
		BoA	115.8	51.41	49.76	27.00	24.04	18.58	13.83
	20	OPTQ	163.1	71.75	64.19	32.83	24.66	20.37	14.41
		BoA	111.1	50.92	48.81	26.96	23.31	19.15	13.80
	50	OPTQ	190.8	69.02	64.99	32.69	24.55	20.13	14.48
		BoA	119.2	51.21	46.68	27.11	23.73	18.96	13.80
	100	OPTQ	168.5	69.56	67.54	33.65	25.25	20.23	14.51
		BoA	116.7	50.69	48.49	27.17	24.09	19.63	13.91
	Mean \pm Stdev	OPTQ	178.2 \pm 12	71.03 \pm 1.7	65.00 \pm 1.5	33.28 \pm 0.53	24.75 \pm 0.33	20.24 \pm 0.14	14.46 \pm 0.039
		BoA	116.2 \pm 3.1	51.66 \pm 1.4	48.53 \pm 1.1	26.96 \pm 0.24	23.64 \pm 0.46	19.11 \pm 0.38	13.83 \pm 0.045

⁶Tables 2 to 9 present the results for seed 0.

(b) INT3 Quantization

Dataset	Seed	Method	125M	350M	1.3B	2.7B	6.7B	13B	30B
WikiText-2	0	OPTQ	38.74	26.31	16.70	14.01	11.91	10.85	9.911
		BoA	33.68	24.69	15.93	13.43	11.53	10.58	9.826
	10	OPTQ	40.72	26.33	16.99	13.97	11.89	10.84	9.881
		BoA	34.30	24.74	16.15	13.43	11.43	10.59	9.756
	20	OPTQ	38.72	26.74	17.17	13.89	11.98	10.94	9.941
		BoA	34.24	24.94	16.02	13.32	11.66	10.51	9.791
	50	OPTQ	37.72	26.55	16.93	14.08	11.86	10.92	9.769
		BoA	34.73	25.00	16.19	13.44	11.44	10.54	9.768
	100	OPTQ	38.37	26.10	16.97	14.27	11.89	10.88	9.840
		BoA	34.51	24.92	16.14	13.72	11.49	10.52	9.847
	Mean ± Stdev	OPTQ	38.85 ± 1.1	26.41 ± 0.24	16.95 ± 0.17	14.04 ± 0.14	11.91 ± 0.044	10.89 ± 0.045	9.868 ± 0.067
		BoA	34.29 ± 0.39	24.86 ± 0.13	16.09 ± 0.11	13.47 ± 0.15	11.51 ± 0.094	10.55 ± 0.036	9.798 ± 0.038
PTB	0	OPTQ	57.62	39.35	24.77	21.53	17.56	15.68	14.56
		BoA	48.50	36.83	23.53	20.33	16.86	15.21	14.50
	10	OPTQ	55.56	39.13	25.19	21.60	17.19	15.66	14.66
		BoA	48.37	36.81	23.35	20.27	16.71	15.13	14.50
	20	OPTQ	56.22	39.97	25.47	21.42	17.24	15.67	14.60
		BoA	47.01	37.07	23.31	20.22	16.68	15.16	14.54
	50	OPTQ	56.68	39.69	24.94	21.44	17.36	15.74	14.52
		BoA	51.05	37.14	23.69	20.19	16.76	15.22	14.46
	100	OPTQ	52.15	38.75	25.13	21.32	17.44	15.79	14.53
		BoA	48.66	36.52	23.50	19.93	16.77	15.21	14.46
	Mean ± Stdev	OPTQ	55.65 ± 2.1	39.38 ± 0.48	25.10 ± 0.26	21.46 ± 0.11	17.36 ± 0.15	15.71 ± 0.057	14.57 ± 0.058
		BoA	48.72 ± 1.5	36.87 ± 0.24	23.48 ± 0.15	20.19 ± 0.16	16.75 ± 0.068	15.19 ± 0.038	14.49 ± 0.035
C4	0	OPTQ	33.90	26.68	18.18	16.10	13.60	12.62	11.76
		BoA	31.12	25.39	17.74	15.83	13.34	12.52	11.75
	10	OPTQ	34.16	26.68	18.19	16.07	13.60	12.63	11.76
		BoA	31.72	25.34	17.72	15.70	13.34	12.52	11.74
	20	OPTQ	34.07	26.88	18.19	16.07	13.58	12.62	11.75
		BoA	31.29	25.46	17.72	15.73	13.33	12.53	11.74
	50	OPTQ	33.68	26.80	18.16	16.06	13.60	12.67	11.76
		BoA	31.11	25.40	17.73	15.73	13.37	12.54	11.74
	100	OPTQ	33.80	26.57	18.20	16.12	13.61	12.66	11.76
		BoA	31.38	25.41	17.75	15.70	13.36	12.55	11.75
	Mean ± Stdev	OPTQ	33.92 ± 0.20	26.72 ± 0.12	18.18 ± 0.015	16.08 ± 0.026	13.60 ± 0.014	12.64 ± 0.023	11.76 ± 0.0045
		BoA	31.32 ± 0.25	25.40 ± 0.044	17.73 ± 0.013	15.74 ± 0.053	13.35 ± 0.016	12.53 ± 0.012	11.75 ± 0.0053

D Pseudocode for OPTQ

In this appendix, we provide the pseudocode of the conventional OPTQ (Frantar et al., 2023), which is omitted in the main manuscript due to the page limitation.

Algorithm 2 OPTQ

Input: weights \mathbf{W} , Hessian information \mathbf{U}_{col} , pre-determined step size \mathbf{S} , and blocksize B

```
1: def OPTQ( $\mathbf{W}$ ,  $\mathbf{U}_{\text{col}}$ ,  $\mathbf{S}$ ,  $B = 128$ )
2:   Initialize quantized output:  $\mathbf{Q} \leftarrow \mathbf{0}_{d_{\text{row}} \times d_{\text{col}}}$ 
3:   Initialize total quantization errors:  $\mathbf{E}_{\text{total}} \leftarrow \mathbf{0}_{d_{\text{row}} \times d_{\text{col}}}$ 
4:   Initialize block quantization errors:  $\mathbf{E}_{\text{block}} \leftarrow \mathbf{0}_{d_{\text{row}} \times B}$ 
5:   for  $i = 0, B, 2B, \dots$  do
6:     for  $j = i, \dots, i + B - 1$  do
7:       Quantize the  $j$ -th column:  $\mathbf{Q}_{:,j} \leftarrow \text{quant}(\mathbf{W}_{:,j}, \mathbf{S})$ 
8:       Estimate quantization error:  $[\mathbf{E}_{\text{block}}]_{:,j-i} \leftarrow (\mathbf{W}_{:,j} - \mathbf{Q}_{:,j}) / [\mathbf{U}_{\text{col}}]_{j,j}$ 
9:       Update weights in block:  $\mathbf{W}_{:,j:i+B} \leftarrow \mathbf{W}_{:,j:i+B} - [\mathbf{E}_{\text{block}}]_{:,j-i} \cdot [\mathbf{U}_{\text{col}}]_{j,j:(i+B)}$ 
10:    end for
11:    Update all remaining weights:  $\mathbf{W}_{:,i+B} \leftarrow \mathbf{W}_{:,i+B} - \mathbf{E}_{\text{block}} \cdot [\mathbf{U}_{\text{col}}]_{i:(i+B), (i+B)}$ 
12:    Save block quantization errors:  $[\mathbf{E}_{\text{total}}]_{:,i:i+B} \leftarrow \mathbf{E}_{\text{block}}$ 
13:  end for
```

Output: quantized weights \mathbf{Q} , quantization error $\mathbf{E}_{\text{total}}$
